ENGINEERING COMPUTATIONS, VOL. 12, 209–228 (1995)

CONTRIBUTED Papers

DISCRETIZATION INFLUENCE IN STRAIN-SOFTENING PROBLEMS

L. J. SLUYS, M. CAUVERN AND R. DE BORST†

Department of Civil Engineering, Delft University of Technology, PO Box 5048, 2600 GA Delft, The Netherlands

ABSTRACT

The dispersive behaviour of waves in softening problems is analysed. Attention is focused on the influence of the numerical scheme on the dispersion characteristics in the process of localization of deformation. Distinction has been made between softening models defined in a standard plasticity framework and in a gradient-dependent plasticity theory. Waves in a standard softening plasticity continuum do not disperse but due to spatial discretization dispersion is introduced which results in a mesh size dependent length scale effect. On the other hand, wave propagation in a gradient-dependent softening plasticity continuum is dispersive. By carrying out the dispersion analysis on the discretized system the influence of numerical dispersion on material dispersion can be quantified which enables us to determine the accuracy for the solution of the localization zone. For a modelling with and without the inclusion of strain gradients accuracy considerations with respect to mass discretization, finite element size, time integration scheme and time step have been carried out.

KEY WORDS Dispersion analysis Softening plasticity model

INTRODUCTION

A large number of engineering materials including metals, polymers, soils, concrete and rock are classified as softening materials. These materials show a reduction of the load-carrying capacity accompanying by increasing localized deformations after reaching the limit load. For the continuum modelling of softening behaviour the standard plasticity framework is widely used. However, the use of standard softening plasticity models results in an ill-posed problem with imaginary wave speeds. As a consequence, localization of deformation stays confined to a zone of zero thickness. The finite element solution tries to capture the localization zone of zero thickness which results in mesh sensitivity. Inclusion of higher-order spatial derivatives in the constitutive equations has been proposed[1,2,9–11] to rephrase standard continuum plasticity and to avoid a spurious solution for the localization zone and an excessive mesh dependence. In this paper, the standard softening plasticity modelling as well as the gradient-dependent softening plasticity modelling will be assessed with respect to their capabilities in localization problems.

A dispersion analysis will be used to demonstrate the features of the softening plasticity model with and without the inclusion of higher-order strain gradients. Eringen[4,5] showed in his work

†Also at Department of Mechanical Engineering, Eindhoven University of Technology.

0264–4401/95/030209–20$2.00

Received September 1993

on non-local elasticity that waves in a higher-order continuum are dispersive. Here, it will be shown for softening problems what ill-posedness of the standard plasticity problem means in terms of its dispersive characteristics. For the gradient model it is known from earlier work[12,13] that real frequencies and dispersive properties are important for the simulation of localization zones that have a finite thickness as observed for shear bands in metals, soils and rock and for fracture process zones in concrete. The width of the localization zone is determined by the critical mode that a gradient-dependent medium can transmit which is set by the length scale of the model.

This paper is primarily concerned with the discretization influence in softening problems. By carrying out the dispersion analysis on the discretized system of equations additional dispersion effects introduced by the numerical scheme can be quantified. This dispersion contribution by spatial and temporal discretization affects the solution for the localization zone. This holds true if the underlying material is a non-dispersive medium as in standard plasticity but also if the material shows dispersion as a physical quantity as in gradient-dependent plasticity. Accuracy considerations with respect to mass discretization, time integration scheme, time step and finite element size have been carried out.

SOFTENING PLASTICITY AND GRADIENT-DEPENDENT SOFTENING PLASTICITY

We consider an initial boundary value problem in one spatial direction. The governing equations for motion and continuity can then be stated as:

$$\frac{\partial \sigma}{\partial x} = \rho \frac{\partial^2 u}{\partial t^2} \tag{1}$$

and

$$\varepsilon = \frac{\partial u}{\partial x} \tag{2}$$

with ρ the mass density, u the displacement, σ and ε stress and strain and x and t spatial and temporal variables, respectively. For the constitutive relation we shall use a plasticity formalism, so that the strain ε is decomposed into an elastic contribution ε^e and a plastic contribution ε^p:

$$\varepsilon = \varepsilon^e + \varepsilon^p \tag{3}$$

The elastic component is related to the stress σ via a bijective relation:

$$\sigma = E\varepsilon^e \tag{4}$$

with E Young's modulus. The strain-softening model is assumed to have the following format:

$$\sigma = f(\varepsilon^p) \tag{5}$$

or in a rate form:

$$\dot{\sigma} = h\dot{\varepsilon}^p \tag{6}$$

with

$$h = \frac{\partial f}{\partial \varepsilon^p} \tag{7}$$

a constant negative value, representing linear strain-softening behaviour and a superimposed dot denoting differentiation with respect to time. On the other hand, the gradient-dependent strain-softening model is given according to the form:

$$\sigma = f(\varepsilon^p, \partial^2 \varepsilon^p / \partial x^2) \tag{8}$$

which in rate form yields:

$$\dot{\sigma} = h\dot{\varepsilon}^p - \bar{c} \frac{\partial^2 \dot{\varepsilon}^p}{\partial x^2} \tag{9}$$

where in the analyses presented here,

$$\bar{c}=\frac{-\partial f}{\partial(\partial^2\varepsilon^p/\partial x^2)} \tag{10}$$

has also been assumed to be a constant.

Combination of (1)–(4) and (6) results in the wave equation for a one-dimensional softening plasticity element:

$$\rho\frac{\partial^2 u}{\partial t^2}-\frac{hE}{h+E}\frac{\partial^2 u}{\partial x^2}=0 \tag{11}$$

If we combine (1)–(4) with (9) we obtain the wave equation for a one-dimensional gradient-dependent softening plasticity element:

$$\frac{\bar{c}}{h+E}\left(E\frac{\partial^4 u}{\partial x^4}-\rho\frac{\partial^4 u}{\partial x^2\partial t^2}\right)+\rho\frac{\partial^2 u}{\partial t^2}-\frac{hE}{h+E}\frac{\partial^2 u}{\partial x^2}=0 \tag{12}$$

If $\bar{c}\to 0$ the wave equation for the softening plasticity element (11) is recovered.

DISPERSION

For a dispersion analysis we consider a single harmonic wave which propagates through a one-dimensional element of the form:

$$u(x,t)=Ae^{i(kx-\omega t)} \tag{13}$$

The frequency ω is a function of the wave number k

$$\omega=f(k) \tag{14}$$

The function $f(k)$ is determined by the particular system under consideration. A system is considered to be dispersive if[1,5]:

$$f'(k)\neq 0 \tag{15}$$

in which a prime denotes differentiation with respect to k.

If condition (15) is true the phase speed:

$$c=\frac{\omega}{k} \tag{16}$$

is not the same for every wave number k and modes represented by its wave number travel at different speeds and will therefore disperse. Finally, we adopt the standard definitions for the wave length:

$$\lambda=\frac{2\pi}{k} \tag{17}$$

and the period:

$$T=\frac{2\pi}{\omega} \tag{18}$$

For a linear-elastic system ($\varepsilon^p=0$) (14) has the non-dispersive form:

$$\omega=c_e k \tag{19}$$

with $c_e=\sqrt{E/\rho}$ the so-called bar wave velocity. For the softening plasticity system, governed by

(11), substitution of (13) yields:

$$\omega = ic_e k\sqrt{\frac{-h}{E+h}} \tag{20}$$

which means that all modes, represented by its wave number k, become stationary waves with the same imaginary frequency and phase velocity and the system is non-dispersive. Basically, in the softening plasticity system the imaginary value of the angular frequency ω represents a real growth coefficient and the solution according to (13) is an exponential function in time. For this reason in the next section a growth coefficient will be introduced as $\omega_r = -i\omega$.

Turning now our attention to gradient-dependent plasticity we substitute the harmonic wave solution (13) into (12). The dispersion relation for the gradient-dependent softening plasticity system can then be elaborated as:

$$\omega = c_e k\sqrt{\frac{h+\bar{c}k^2}{E+h+\bar{c}k^2}} \tag{21}$$

Now, the frequency is a real function of wave number k if

$$k \geqslant \sqrt{-\frac{h}{\bar{c}}} \tag{22}$$

or using (17):

$$\lambda \leqslant 2\pi l \tag{23}$$

with

$$l = \sqrt{-\frac{\bar{c}}{h}} \tag{24}$$

Equation (22) states that there exists a cut-off value for k. This value of k corresponds to the mode with the largest wave length that the gradient-dependent softening system can transmit. Above this value for k all frequencies are real.

The parameter l is defined as the length scale parameter in the gradient-dependent plasticity model. Since the gradient constant $\bar{c}$ has entered the dispersion relation $f''(k) \neq 0$ and wave propagation in the gradient-dependent plasticity system is dispersive. The dispersion curves have been plotted in *Figure 1a* for the linear-elastic system, the softening plasticity system and the gradient-dependent softening plasticity system. In *Figure 1b* the corresponding phase velocity–wave number (c–k) curve is shown. In the *Figures 1a* and *1b* the bar wave velocity $c_e = 1000$ m/s, the Young's modulus $E = 20{,}000$ N/mm^2, the softening modulus $h = -0.1E$ and the gradient constant $\bar{c} = 50{,}000$ N. The values for h and $\bar{c}$ imply a length scale parameter $l = 5.0$ mm.

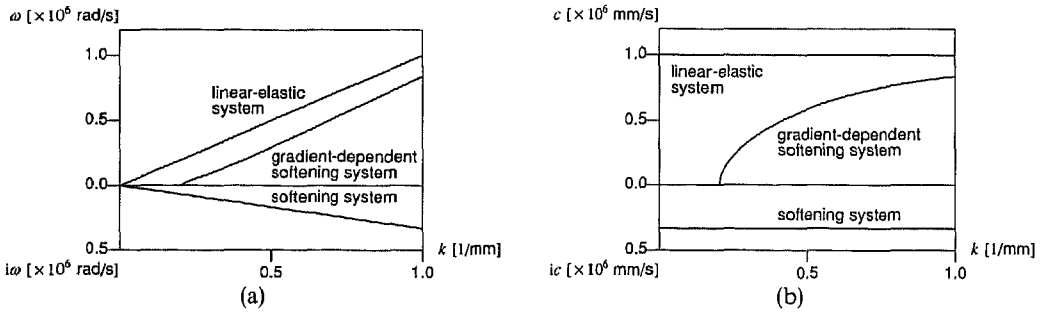

Figure 1 Continuum dispersion curves for a linear elastic, softening and gradient-dependent softening system. (a) Frequency *versus* wave number; (b) phase velocity versus wave number

Dispersion in a softening system as described in this paper is closely related to the problem of localization of deformation. As a result of softening localization of deformation may occur and the behaviour of localized zones is very much dependent on the dispersive characteristics of the material[12]. For the softening plasticity system the inability of the material to transmit waves with a real frequency (and phase velocity) causes the strains to localize in zones of zero thickness. As soon as softening occurs localization of deformation is trapped and the zone cannot extend. It will be demonstrated later that the numerical solution of the localization zone in the softening plasticity system belongs to a stationary wave with frequency and phase velocity equal to zero. The dispersion contribution due to spatial discretization causes the frequency to reach a real zero value. The mesh-dependent solution for the localization zone corresponds to this stationary wave and its wave length λ is equal to the width of the zone, namely a one finite element wide zone (in case of constant strain elements).

For the gradient-dependent softening system the fact that waves with real phase velocities disperse has the advantageous consequence that the localization zone can extend and the strain profile in the localization zone can be transformed because different modes travel at different speeds. These features are of pivotal importance to simulate zones of localized deformation with a finite size instead of the zero-thickness solution as obtained for the softening plasticity system. Also for the gradient model the localization zone acts as a stationary wave with frequency and phase velocity equal to zero. For this reason the width of the localization zone w is equal to the lowest-order wave that the gradient-dependent softening system can transmit, i.e. $w=2\pi l$. The width of the localization zone appears as a consequence of the length scale effect and the spurious mesh dependence is removed[13].

In finite element formulations the governing equations for a one-dimensional softening plasticity element ((11)) and for a gradient-dependent softening plasticity element ((12)) are discretized with respect to spatial and temporal variables. As mentioned before, discretization is another source of dispersion (see earlier work[7,14], and is introduced irrespective of the fact whether the underlying material exhibits dispersion of waves (gradient-dependent softening system) or not (softening system). The dispersion contribution of both temporal and spatial discretization will be assessed separately, in the next section, firstly, for the softening plasticity system and, secondly, for the gradient-dependent softening plasticity system.

DISCRETIZATION INFLUENCE IN SOFTENING PLASTICITY

Dispersion contribution by temporal discretization

A general family of time integration algorithms is considered that contains the Hilber–Hughes–Taylor α-method[6] as well as the Newmark-method family[8]:

$$\mathbf{M}\ddot{\mathbf{a}}^{t+\Delta t}+(1+\alpha)\mathbf{K}\mathbf{a}^{t+\Delta t}-\alpha\mathbf{K}\mathbf{a}^{t}=0 \tag{25}$$

$$\mathbf{a}^{t+\Delta t}=\mathbf{a}^{t}+\Delta t\dot{\mathbf{a}}^{t}+\Delta t^{2}[(\tfrac{1}{2}-\beta)\ddot{\mathbf{a}}^{t}+\beta\ddot{\mathbf{a}}^{t+\Delta t}] \tag{26}$$

$$\dot{\mathbf{a}}^{t+\Delta t}=\dot{\mathbf{a}}^{t}+\Delta t[(1-\gamma)\ddot{\mathbf{a}}^{t}+\gamma\ddot{\mathbf{a}}^{t+\Delta t}] \tag{27}$$

with $\ddot{\mathbf{a}}$, $\dot{\mathbf{a}}$ and $\mathbf{a}$ the nodal accelerations, velocities and displacements, respectively. Equations (25)–(27) represent a semi-discrete system with mass matrix $\mathbf{M}$ and stiffness matrix $\mathbf{K}$, which is assumed to be constant over Δt. In this section spatial discretization is ignored and the continuum values for $\mathbf{M}$ and $\mathbf{K}$ will be substituted. The integration parameters α, β and γ determine the stability, accuracy and dissipative properties of the system. Moreover, these parameters have an influence on dispersion, which will be demonstrated in this paper for softening materials. Taking $\alpha=0$ the scheme reduces to the Newmark-method family with $\gamma=\frac{1}{2}$ and $\beta=\frac{1}{4}$ the average acceleration method, $\gamma=\frac{1}{2}$ and $\beta=\frac{1}{12}$ the Fox–Goodwin method and $\gamma=\frac{1}{2}$ and $\beta=0$ the central difference method. Numerical dissipation can be introduced when $\gamma>\frac{1}{2}$, however, from linear-elastic considerations[8] it is known that second-order accuracy is lost in this case. For this reason

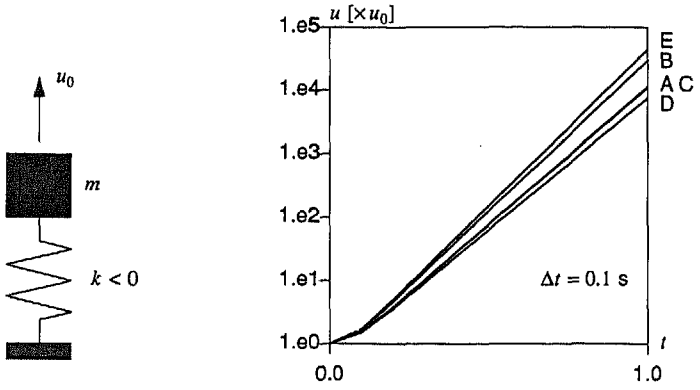

$\omega_r = \sqrt{-k/m} = 10$ rad/s
$u(0) = u_0$, $\dot{u}(0) = 0$

A : exact solution
B : $\alpha = 0$ $\beta = 1/4$ $\gamma = 1/2$
C : $\alpha = 0$ $\beta = 1/12$ $\gamma = 1/2$
D : $\alpha = 0$ $\beta = 0$ $\gamma = 1/2$
E : $\alpha = -0.3$ $\beta = 0.4225$ $\gamma = 0.8$

time step	error B	error C	error D	error E
$\Delta t = 0.05$	2.6623e3	1.4215e1	-1.0614e3	3.9499e3
$\Delta t = 0.025$	5.9454e2	8.9410e-1	-2.8115e2	8.6993e2
$\Delta t = 0.0125$	1.4468e2	5.5981e-2	-7.1343e1	2.1301e2
N	4.1	16.0	3.9	4.1

$\text{error} = \frac{u_{\Delta t} - u}{u_0}$, $N = \frac{u_{\Delta t = 0.025} - u}{u_{\Delta t = 0.0125} - u}$, u = exact displacement at $t = 1.0$ s

Figure 2 Single degree of freedom system with a negative stiffness

Hilber, Hughes and Taylor[6] developed the α-method in which numerical dissipation is introduced via $-\frac{1}{3} < \alpha < 0$ while second-order accuracy can be preserved if $\gamma = \frac{1}{2} - \alpha$ and $\beta = \frac{1}{4}(1-\alpha)^2$.

Before carrying out the dispersion analysis for a one-dimensional strain-softening system that is discretized in the time domain we will discuss results obtained by Xie and Wood[16] and Cauvern[3] for a single degree of freedom system with a negative stiffness, representing softening behaviour. The problem sketched in *Figure 2* has been analysed using abovementioned time integration schemes. The mass is initially displaced over u_0 and the displacement grows exponentially in time according to the analytical solution:

$$u(t) = \tfrac{1}{2}u_0 e^{-\omega_r t} + \tfrac{1}{2}u_0 e^{\omega_r t} \tag{28}$$

The results have been plotted in *Figure 2*. It is obvious that the implicit Newmark-methods and the α-method give an upper bound estimate of growth coefficient ω_r and displacement u, while the explicit central difference scheme underestimates the analytical solution. From the results reported in *Figure 2* Xie and Wood[16] concluded that the average acceleration method ($\gamma = \frac{1}{2}$, $\beta = \frac{1}{4}$) shows $O(\Delta t^2)$ convergence and the Fox–Goodwin scheme ($\gamma = \frac{1}{2}$, $\beta = \frac{1}{12}$) is $O(\Delta t^4)$ accurate. N represents the convergence rate, i.e. a decrease of the time step by a factor 2 results in a decrease of the error by a factor 16.0 for the Fox–Goodwin method and by a factor 4.1 for the average acceleration method.

The abovementioned results can be explained carrying out a dispersion analysis for the softening plasticity problem discretized in the time domain. For the problem governed by wave equation (11) a solution is assumed of the form:

$$u(x,t) = \bar{u}(t)e^{ikx} \tag{29}$$

Substitution of (29) into (11) eliminates the spatial derivative terms yielding:

$$\rho\frac{\partial^2\bar{u}}{\partial t^2}+\frac{hE}{(h+E)}k^2\bar{u}=0 \tag{30}$$

Discrete nodal values are substituted for the displacement function, via $\bar{u}(t)=\mathbf{a}$ and we can rewrite (30) into:

$$M\ddot{\mathbf{a}}+K\mathbf{a}=\mathbf{0} \tag{31}$$

with the continuum values:

$$M=\rho \tag{32}$$

$$K=\frac{hE}{h+E}k^2 \tag{33}$$

By considering the set of equations (25)–(27) at $t-2\Delta t$, $t-\Delta t$, t and $t+\Delta t$ the time derivatives $\dot{a}^{t-\Delta t}$, $\dot{a}^t$, $\ddot{a}^{t-\Delta t}$, $\ddot{a}^t$ and $\ddot{a}^{t+\Delta t}$ can be eliminated and a temporally discretized equation of motion can be derived according to:

$$K(c_0a^{t+\Delta t}-c_1a^t-c_2a^{t-\Delta t}-c_3a^{t-2\Delta t})=\frac{M}{\Delta t^2}(-a^{t+\Delta t}+2a^t-a^{t-\Delta t}) \tag{34}$$

with:

$$c_0=\beta(1+\alpha) \tag{35}$$

$$c_1=\beta\alpha+(1+\alpha)(2\beta-\gamma-\tfrac{1}{2}) \tag{36}$$

$$c_2=(1+\alpha)(\gamma-\beta-\tfrac{1}{2})-\alpha(2\beta-\gamma-\tfrac{1}{2}) \tag{37}$$

$$c_3=-\alpha(\gamma-\beta-\tfrac{1}{2}) \tag{38}$$

Solutions for the strain-softening plasticity system as derived in the previous section show imaginary values for frequency ω and phase velocity c. Hence, we assume non-harmonic solutions of the displacements with a real growth coefficient ω_r:

$$a^t=Ae^{\omega_r t} \tag{39}$$

$$a^{t+\Delta t}=Ae^{\omega_r(t+\Delta t)}=Ae^{\omega_r\Delta t}e^{\omega_r t} \tag{40}$$

$$a^{t-\Delta t}=Ae^{\omega_r(t-\Delta t)}=Ae^{-\omega_r\Delta t}e^{\omega_r t} \tag{41}$$

$$a^{t-2\Delta t}=Ae^{\omega_r(t-2\Delta t)}=Ae^{-2\omega_r\Delta t}e^{\omega_r t} \tag{42}$$

Substitution of the solutions into (34) gives the dispersion relation for the temporally discretized strain-softening system:

$$k^2=\frac{(h+E)}{c_e^2\Delta t^2 h}\frac{D_1}{D_2} \tag{43}$$

with

$$D_1=-e^{\omega_r\Delta t}+2-e^{-\omega_r\Delta t} \tag{44}$$

$$D_2=c_0e^{\omega_r\Delta t}-c_1-c_2e^{-\omega_r\Delta t}-c_3e^{-2\omega_r\Delta t} \tag{45}$$

In *Figure 3* the dispersion relation has been plotted for different values of the time step when the average acceleration method is employed. The curves converge to the continuum dispersion curve if the time step is decreased. For this implicit method we obtain upper bound values of ω_r which agrees with the tendency observed for the single degree of freedom problem in *Figure 2*. In *Figure 4a* the dispersion curve is plotted for different Newmark schemes. It is obvious that the Fox–Goodwin method ($\beta=\frac{1}{12}$) gives the best approximation, while the inclusion of numerical

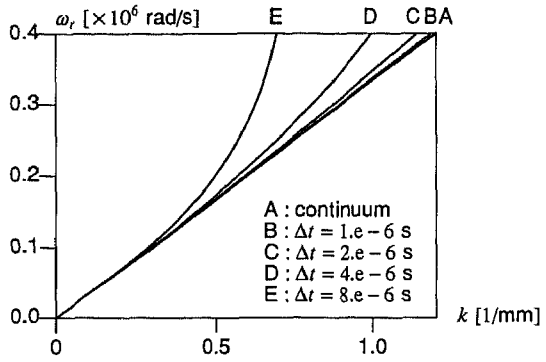

Figure 3 Dispersion curve for temporally discretized softening plasticity system—variation of the time step for the average acceleration method

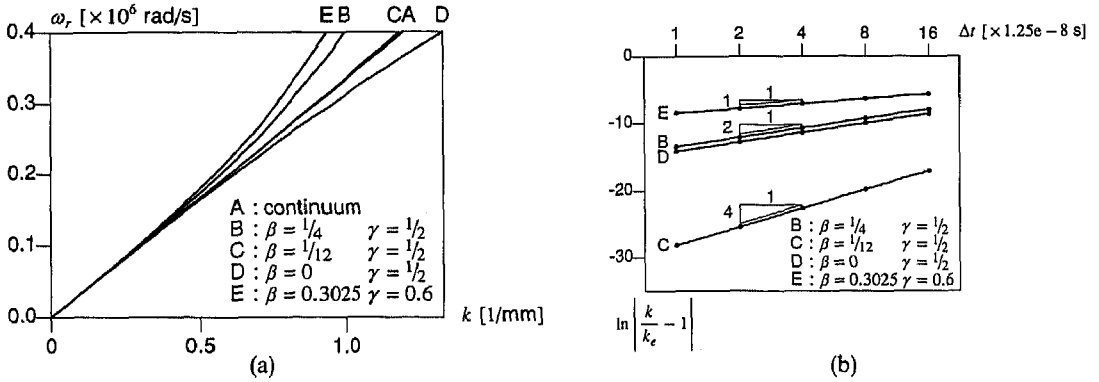

Figure 4 Temporal discretization using the Newmark time integration method. (a) Dispersion curve ($\omega_r - k$) with $\Delta t = 4e-6s$; (b) convergence of time stepping scheme

dissipation by using $\gamma = 0.6$ and $\beta = 0.3025$ reduces the accuracy. The explicit central difference scheme ($\beta = 0$) underestimates ω_r. To determine the exact convergence rate for the Newmark-methods k has been calculated via (43) for $\omega_r = 1.e6$ rad/s (with exact solution $k_e = 1.0$ 1/mm) at different values of the time step. The results, summarized in *Figure 4b*, confirm abovementioned results obtained by Xie and Wood[16] with respect to the convergence rate for the Fox–Goodwin method and the average acceleration method. A $O(\Delta t^4)$-convergence for Fox–Goodwin and a $O(\Delta t^2)$-convergence for average acceleration can be proved with this temporal dispersion analysis. Although the central difference scheme shows a smaller absolute error than the average acceleration method its convergence rate is equal. Newmark with dissipation, i.e. $\gamma = 0.6$ and $\beta = 0.3025$, results in first-order accuracy. The same analysis has been carried out for the α-method schemes and the results are reflected in the *Figures 5a* and *5b*. The results with respect to the accuracy of the Newmark methods and the α-methods have been summarized in *Table 1*.

Dispersion contribution by spatial discretization

The solution for the softening plasticity problem defined by (11) is now taken as:

$$u(x,t) = \bar{u}(x)e^{\omega_r t} \tag{46}$$

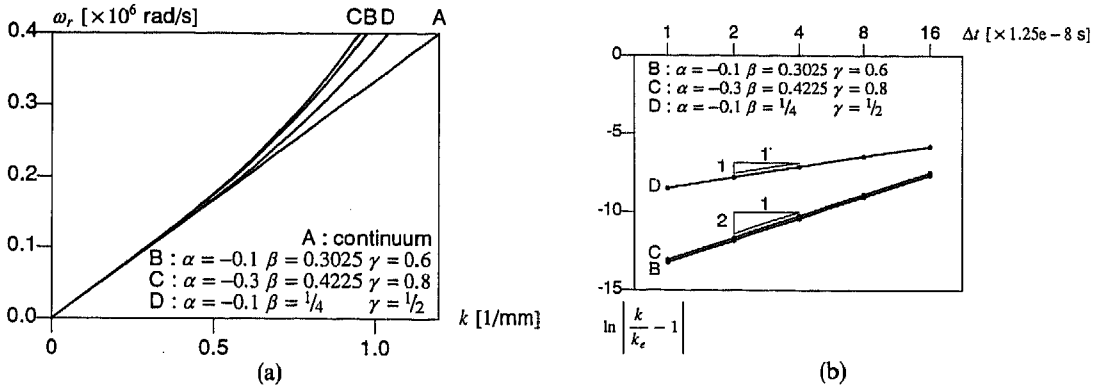

Figure 5 Temporal discretization using the α time integration method. (a) Dispersion curve ($\omega_r - k$) with $\Delta t = 4e-6s$; (b) convergence of time stepping scheme

Table 1 Accuracy of time integration schemes in softening plasticity

Method	α	γ	β	Accuracy
Average acceleration	0	0.5	0.25	$O(\Delta t^2)$
Fox–Goodwin	0	0.5	0.0833	$O(\Delta t^4)$
Central difference	0	0.5	0	$O(\Delta t^2)$
Damped Newmark	0	0.6	0.3025	$O(\Delta t)$
α-Method	−0.1	0.6	0.3025	$O(\Delta t^2)$
α-Method	−0.3	0.8	0.4225	$O(\Delta t^2)$
α-Average acceleration	−0.1	0.5	0.25	$O(\Delta t)$

Substitution of this solution into the equation of motion (1) yields:

$$\frac{\partial \bar{\sigma}}{\partial x} = \rho \omega_r^2 \bar{u} \tag{47}$$

with $\sigma(x,t) = \bar{\sigma}(x) e^{\omega_r t}$. The problem can be described by a weak form of (47) in rate format, into which the elastic stress–strain law (4), the decomposition in strains (3) and the constitutive equation (6) have been substituted. Invoking the divergence theorem and neglecting boundary tractions gives:

$$\rho \omega_r^2 \int_L \delta \dot{\bar{u}} \cdot \dot{\bar{u}} \mathrm{d}L + \frac{hE}{h+E} \int_L \delta \dot{\bar{\varepsilon}} \cdot \dot{\bar{\varepsilon}} \mathrm{d}L = 0 \tag{48}$$

in which $0 < x < L$ and $\bar{\varepsilon} = \partial \bar{u} / \partial x$. A finite element representation is assumed via:

$$\dot{\bar{u}}(x) = \mathbf{H} \dot{\mathbf{a}} \tag{49}$$

$$\dot{\bar{\varepsilon}}(x) = \mathbf{B} \dot{\mathbf{a}} \tag{50}$$

in which matrix **H** contains the interpolation polynomials for the velocity field and **B** = **LH**, with **L** the differential operator matrix. Substitution of (49) and (50) into (48) and assuming that the resulting equation holds for any admissible virtual velocity field $\dot{\mathbf{a}}$ yields:

$$\omega_r^2 \mathbf{M} \dot{\mathbf{a}} + \mathbf{K} \dot{\mathbf{a}} = \mathbf{0} \tag{51}$$

in which

$$\mathbf{M}=\rho\int_L \mathbf{H}^T\mathbf{H}\mathrm{d}L \tag{52}$$

$$\mathbf{K}=\frac{hE}{h+E}\int_L \mathbf{B}^T\mathbf{B}\mathrm{d}L \tag{53}$$

Spatial discretization of (51)–(53) has been done by means of linear bar elements with a two point Gaussian quadrature. The matrices **M** and **K** are given in Appendix A. We assume a mesh with one-dimensional elements of constant length d and consider the spatially discretized equation of motion for node j. In case of a consistent mass we obtain:

$$\frac{\rho\omega_r^2 d}{6}(\dot{a}_{j-1}+4\dot{a}_j+\dot{a}_{j+1})+\frac{hE}{h+E}\frac{1}{d}(-\dot{a}_{j-1}+2\dot{a}_j-\dot{a}_{j+1})=0 \tag{54}$$

while using a lumped or a higher-order mass matrix similar expressions ensue (cf. Appendix A). In contrast to the time discretization analysis a set of harmonic solutions is possible for (54) because the wave number k remains real. We assume a solution at node j and the adjacent nodes of the form:

$$\dot{a}_j=A\mathrm{e}^{\mathrm{i}kx} \tag{55}$$

$$\dot{a}_{j-1}=A\mathrm{e}^{\mathrm{i}k(x-d)}=A(\cos kd-i\sin kd)\mathrm{e}^{\mathrm{i}kx} \tag{56}$$

$$\dot{a}_{j+1}=A\mathrm{e}^{\mathrm{i}k(x+d)}=A(\cos kd+i\sin kd)\mathrm{e}^{\mathrm{i}kx} \tag{57}$$

Substitution of (55)–(57) in the discretized equation of motion gives the dispersion relation for the spatially discretized softening plasticity system:

$$\omega_r=\frac{c_e}{d}\sqrt{\frac{-h}{(h+E)}\frac{K_d}{M_d}} \tag{58}$$

or in terms of the imaginary phase velocity:

$$c=i\frac{c_e}{kd}\sqrt{\frac{-h}{(h+E)}\frac{K_d}{M_d}} \tag{59}$$

in which:

$$K_d=2(1-\cos kd) \tag{60}$$

and:

$$M_d=\tfrac{1}{3}(2+\cos kd) \tag{61}$$

for a consistent mass matrix,

$$M_d=1 \tag{62}$$

for a lumped mass matrix and

$$M_d=\tfrac{1}{6}(5+\cos kd) \tag{63}$$

for a higher-order mass matrix. The higher-order mass matrix is obtained by averaging the lumped and the consistent mass matrices.

The dispersion relation (58) shows that ω_r is not only dependent on k but also on the finite element size d, the mass distribution M_d and, of course, the type of element that has been used. For a consistent mass distribution the ω_r-k curve is plotted in *Figure 6a* for different sizes of the finite element. Convergence to the continuum dispersion curve occurs upon mesh refinement ($d\to 0$). An upper bound estimate of the growth coefficient ω_r is obtained if we use a consistent

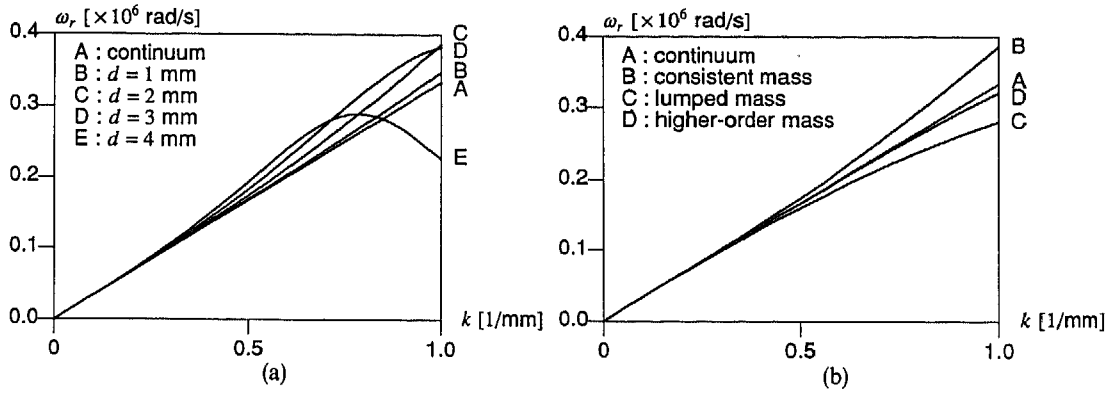

Figure 6 Spatial discretization of softening plasticity system. (a) Dispersion curve ($\omega_r - k$)—variation of d using a consistent mass matrix; (b) dispersion curve ($\omega_r - k$)—variation of mass discretization using $d = 2$ mm

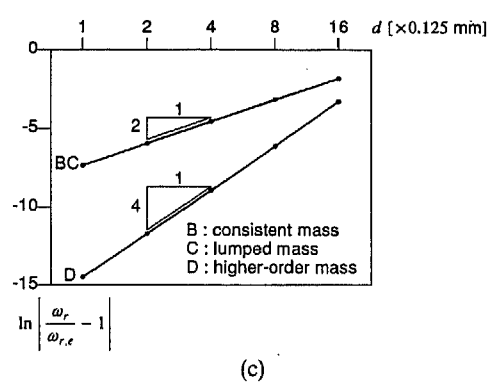

Figure 6 Spatial discretization of softening plasticity system. (c) Convergence of mass discretization

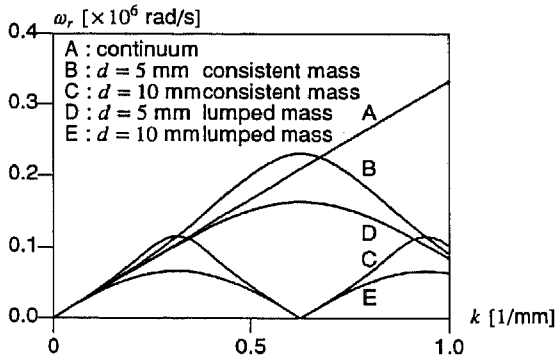

Figure 7 Spatial discretization of softening plasticity system—influence of finite element size d and mass distribution on cut-off value for ω_r

mass matrix. On the other hand, as shown in *Figure 6b*, an analysis with a lumped mass matrix results in a lower bound approximation, while the higher-order mass matrix gives the best performance, even for higher wave numbers (smaller wave lengths). The exact convergence rate for the different mass discretizations has been determined by variation of finite element size d. In *Figure 6c* ω_r has been calculated via (58) for $k = 1.0$ 1/mm and is compared with the exact value $\omega_{r,e}$. The higher-order mass matrix is 4th-order accurate while the consistent and the lumped mass matrix give the same error and are 2nd-order accurate. It is observed in *Figures 6a* and *6b* that the deviation between the curves obtained by spatial discretization and the continuum dispersion curve increases for higher wave numbers (smaller wave lengths). This implies that the accuracy of the finite element solution rapidly reduces when the wave length is of the same order as the finite element size, which is in fact a trivial result. In *Figure 7* it is demonstrated that this inaccuracy leads to cut-off values for ω_r. The growth coefficient ω_r reaches a maximum value, which decreases when a smaller finite element size is taken, cf. $d = 5$ mm *versus* $d = 10$ mm. Use of a lumped mass matrix results in a smaller cut-off value for ω_r in comparison with use of a consistent mass matrix. The existence of a cut-off value for ω_r reflects the fact that there is a limit to the amount of unstable behaviour that a mesh can resolve.

Finally, in *Figure 8* the imaginary phase velocity c has been plotted against wave number k. Although the phase velocity has no physical meaning because in the continuum formulation

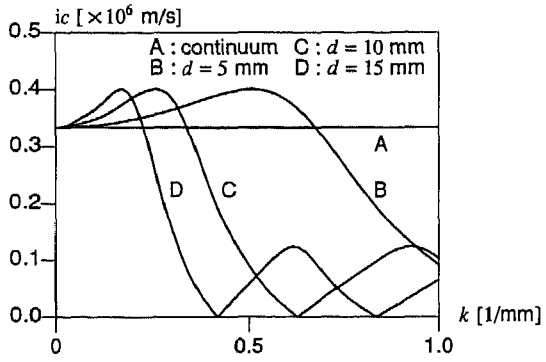

Figure 8 Spatial discretization of softening plasticity system—influence of finite element size on imaginary phase velocity using a consistent mass matrix

((20)) it has the same imaginary value for every mode, the influence of spatial discretization causes the phase velocity to become dependent on k and according to (59) reaches zero (real!) values if:

$$1-\cos kd=0 \tag{64}$$

which is satisfied if the wavelength $\lambda=d$. In numerical solutions of the softening plasticity system we obtain a one-element-wide localization zone in case of constant strain elements. Apparently the localization zone belongs to a stationary wave with a wave length equal to the finite element size and a non-imaginary phase velocity equal to zero. In conclusion, the analytical solution of the localization zone shows an imaginary wave effect, while the numerical solution, due to a regularizing contribution of the spatial discretization, corresponds to a real stationary wave with a wave length set by the finite element mesh.

DISCRETIZATION INFLUENCE IN GRADIENT-DEPENDENT SOFTENING PLASTICITY

Dispersion contribution by temporal discretization

In contrast to the softening system described above, the gradient-dependent softening system exhibits dispersion of waves as a consequence of material behaviour. By carrying out the dispersion analysis, in fact, the interaction between physical and numerical dispersion is examined. For the problem governed by (12) a solution according to (29) is assumed, which gives:

$$\rho\frac{\partial^2\bar{u}}{\partial t^2}+\frac{Ek^2(\bar{c}k^2+h)}{\bar{c}k^2+h+E}\bar{u}=0 \tag{65}$$

which in discrete format reads

$$M\ddot{\mathbf{a}}+K\mathbf{a}=\mathbf{0} \tag{66}$$

with

$$M=\rho \tag{67}$$

$$K=\frac{Ek^2(\bar{c}k^2+h)}{\bar{c}k^2+h+E} \tag{68}$$

Equations (34)–(37), discretized in the time domain for the Newmark-method family and the

α-method, are also valid for the gradient-dependent softening system, of course K now given by (68). Solutions for (66) now are harmonic according to:

$$a^t = Ae^{i\omega t} \tag{69}$$

$$a^{t+\Delta t} = Ae^{i\omega(t+\Delta t)} = A(\cos\omega\Delta t + i\sin\omega\Delta t)e^{i\omega t} \tag{70}$$

$$a^{t-\Delta t} = Ae^{i\omega(t-\Delta t)} = A(\cos\omega\Delta t - i\sin\omega\Delta t)e^{i\omega t} \tag{71}$$

$$a^{t2\Delta t} = Ae^{i\omega(t-2\Delta t)} = A(\cos 2\omega\Delta t - i\sin 2\omega\Delta t)e^{i\omega t} \tag{72}$$

Substitution of the set of solutions into (34) gives the dispersion relation with real and imaginary components. It appears that the real part offers the non-trivial solution by:

$$k^2 = \tfrac{1}{2}\left(\frac{D_1}{c_e^2\Delta t^2} - \frac{hD_2}{\bar{c}}\right) + \tfrac{1}{2}\left(\frac{D_1^2}{c_e^4\Delta t^4} + \frac{h^2D_2^2}{\bar{c}^2} + \frac{2(2E+h)D_1D_2}{c_e^2\Delta t^2\bar{c}}\right)^{1/2} \tag{73}$$

in which:

$$D_1 = 2(1-\cos\omega\Delta t) \tag{74}$$

$$D_2 = (c_0 - c_2)\cos\omega\Delta t - c_3\cos 2\omega\Delta t - c_1 \tag{75}$$

and the real phase velocity follows from $c^2 = \omega^2/k^2$.

In *Figure 9a* the dispersion curve has been plotted for different time integration schemes. As for the standard softening plasticity system the Fox–Goodwin method shows the best performance for gradient-dependent softening plasticity. It is remarkable that the Fox–Goodwin method, although the method is implicit on the basis of linear elastic considerations, gives an upper bound approximation of the continuum dispersion curve just like the central difference scheme. The average acceleration method and the α-method underestimate the frequency ω leading to elongated periods T. In *Figure 9b* the rate of convergence is plotted for the time integration schemes by means of the difference with the continuum solution at $k_e = 1.0$ 1/mm. The results are exactly the same as for the softening plasticity system, i.e. the Fox–Goodwin method exactly reaches $O(\Delta t^4)$ accuracy while the average acceleration method, the α-method and the central difference scheme perform $O(\Delta t^2)$ accurate. So the conclusions from *Table 1* for the softening plasticity system also hold true for the gradient-dependent softening plasticity system.

As discussed earlier softening is the driving force for localization of deformation and the localization zone is represented by a stationary wave with frequency ω and phase velocity c both equal to zero. In *Figures 9a* and *10*, in which the phase velocity is plotted against the wave

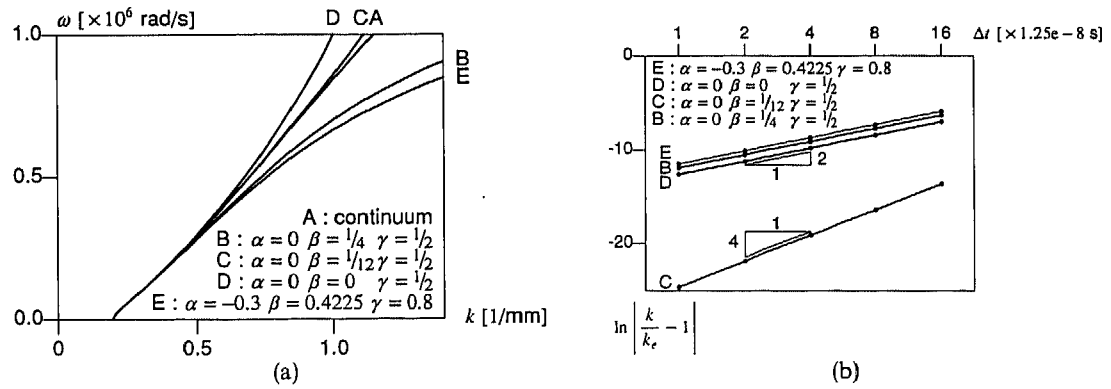

Figure 9 Dispersion curve for temporally discretized gradient-dependent softening plasticity system. (a) Dispersion curve ($\omega_r - k$)—variation of time integration scheme using $\Delta t = 2e-6$s; (b) convergence of time stepping scheme

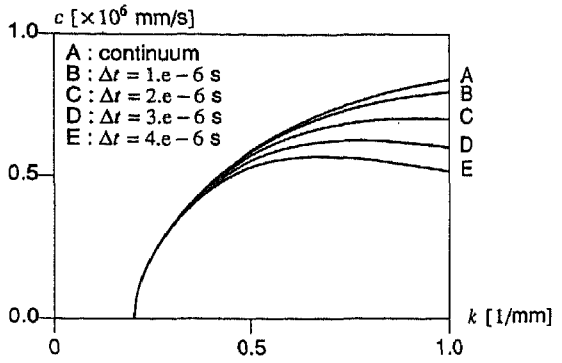

Figure 10 Dispersion curve for temporally discretized gradient-dependent softening plasticity system—real phase velocities upon variation of the time step for average acceleration method

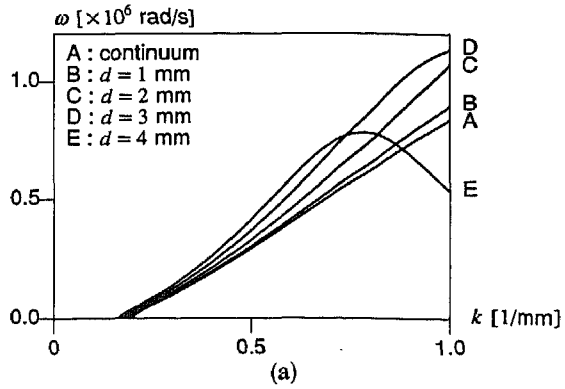

Figure 11 Spatial discretization of gradient-dependent softening plasticity system. (a) Dispersion curve ($\omega - k$)—variation of d using a consistent mass matrix

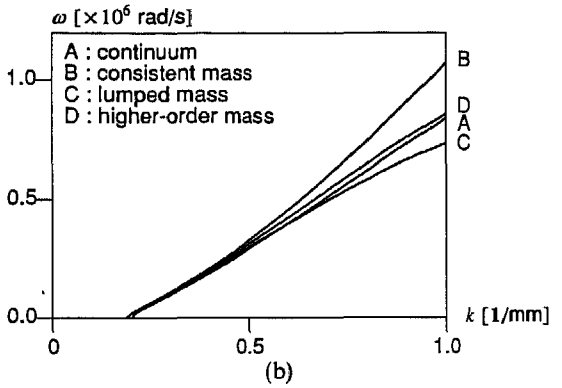

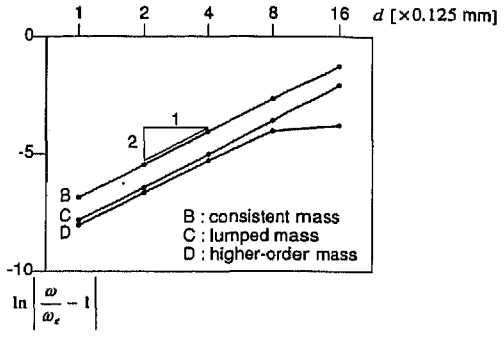

Figure 11 Spatial discretization of gradient-dependent softening plasticity system. (b) dispersion curve $\omega - k$)—variation of mass discretization using $d = 2$ mm (c) Convergence of mass discretization

number for the average acceleration scheme, the stationary wave is reflected by the cut-off value for wave number $k = \sqrt{-h/\bar{c}}$. It appears that this value is not affected by the time integration scheme (*Figure 9a*) or the time step (*Figure 10*).

Dispersion contribution by spatial discretization

The problem with the application of standard algorithms for elastoplastic solids for the gradient-dependent plasticity formulation is that (9) is a partial differential equation. To solve the problem numerically Mühlhaus and Aifantis[10] and de Borst and Mühlhaus[2] have proposed to consider the plastic strain ε^p as an independent unknown in addition to the displacement. For this purpose we assume harmonic solutions of the form:

$$u(x,t) = \bar{u}(x)e^{i\omega t} \tag{76}$$

$$\varepsilon^p(x,t) = \bar{\varepsilon}^p(x)e^{i\omega t} \tag{77}$$

The problem can be described by a weak form of the rate equation of motion (1) and the constitutive rate equation (9), in which the solution (76)–(77) is substituted and $\dot{\bar{\sigma}} = E(\dot{\bar{\varepsilon}} - \dot{\bar{\varepsilon}}^p)$:

$$-\rho\omega^2 \int_L \delta\dot{\bar{u}} \cdot \dot{\bar{u}} \mathrm{d}L + \int_L \delta\dot{\bar{\varepsilon}} \cdot E(\dot{\bar{\varepsilon}} - \dot{\bar{\varepsilon}}^p)\mathrm{d}L = 0 \tag{78}$$

$$\int_L \delta\dot{\bar{\varepsilon}}^p \left[E(\dot{\bar{\varepsilon}} - \dot{\bar{\varepsilon}}^p) - h\dot{\bar{\varepsilon}}^p + \bar{c}\frac{\partial^2 \dot{\bar{\varepsilon}}^p}{\partial x^2} \right] \mathrm{d}L = 0 \tag{79}$$

and, again, the divergence theorem has been applied while the boundary tractions were neglected. We assume a finite element representation of (78) and (79) via:

$$\dot{u}(x) = \mathbf{H}\dot{\mathbf{a}} \tag{80}$$

$$\dot{\bar{\varepsilon}}(x) = \mathbf{B}\dot{\mathbf{a}} \tag{81}$$

$$\dot{\bar{\varepsilon}}^p(x) = \mathbf{h}^{\mathrm{T}}\dot{\mathbf{e}} \tag{82}$$

$$\frac{\partial^2 \dot{\bar{\varepsilon}}^p(x)}{\partial x^2} = \mathbf{p}^{\mathrm{T}}\dot{\mathbf{e}} \tag{83}$$

in which $\dot{\mathbf{e}}$ are the nodal plastic strain rates. An important issue is now the order of interpolation of the variables $\dot{u}$ and $\dot{\bar{\varepsilon}}^p$. While C^0-interpolants suffice for $\dot{u}$, the presence of a second spatial derivative of $\dot{\bar{\varepsilon}}^p$ requires C^1-continuous shape functions. In the numerical analysis presented here, Hermitian functions have been used for $\mathbf{h}$ for this purpose. Because of that the nodal gradients of the plastic strain rate $\mathrm{d}\dot{\mathbf{e}}$ enter the equations as additional variables. $\mathbf{p}$ is calculated by differentiating the polynomials of $\mathbf{h}$ twice. The matrices $\mathbf{H}$ and $\mathbf{B}$ are standard and $\mathbf{h}$ and $\mathbf{p}$ are given in Appendix B.

Substitution of (80)–(83) into (78) and (79) yields:

$$-\omega^2 \mathbf{M}_{aa}\ddot{\mathbf{a}} + \mathbf{K}_{aa}\dot{\mathbf{a}} - \mathbf{K}_{ae}\dot{\mathbf{e}} = \mathbf{0} \tag{84}$$

$$\mathbf{K}_{ea}\dot{\mathbf{a}} + \mathbf{K}_{ee}\dot{\mathbf{e}} = \mathbf{0} \tag{85}$$

in which

$$\mathbf{M}_{aa} = \rho \int_L \mathbf{H}^{\mathrm{T}}\mathbf{H}\mathrm{d}L \tag{86}$$

$$\mathbf{K}_{aa} = E \int_L \mathbf{B}^{\mathrm{T}}\mathbf{B}\mathrm{d}L \tag{87}$$

$$\mathbf{K}_{ae} = E \int_L \mathbf{B}^{\mathrm{T}}\mathbf{h}^{\mathrm{T}}\mathrm{d}L \tag{88}$$

$$\mathbf{K}_{ea} = E \int_L \mathbf{h}\mathbf{B}\mathrm{d}L \tag{89}$$

$$\mathbf{K}_{ee} = \int_L [-(h+E)\mathbf{h}^{\mathrm{T}}\mathbf{h} + \bar{c}\mathbf{h}\mathbf{p}^{\mathrm{T}}]\mathrm{d}L \tag{90}$$

The matrices (86)–(90) have been determined for a bar element with a two-point quadrature rule as described in Appendix B. Again, we assume a mesh with elements of constant length d and considering (84) and (85) for node j results in the following three equations with the unknowns $\dot{a}$, $\dot{e}$ and $\mathrm{d}\dot{e}$:

$$-\frac{\rho\omega^2 d}{16}(3\ddot{a}_{j-1} + 10\ddot{a}_j + 3\ddot{a}_{j+1}) + \frac{E}{d}(-\dot{a}_{j-1} + 2\dot{a}_j - \dot{a}_{j+1}) -$$

$$\frac{E}{2}(\dot{e}_{j-1} - \dot{e}_{j+1}) - \frac{Ed}{32}(3\mathrm{d}\dot{e}_{j-1} - 6\mathrm{d}\dot{e}_j + 3\mathrm{d}\dot{e}_{j+1}) = 0 \tag{91}$$

$$\frac{E}{2}(-\dot{a}_{j-1}+\dot{a}_{j+1})-\frac{(h+E)d}{1024}(135\dot{e}_{j-1}+754\dot{e}_j+135\dot{e}_{j+1})-\frac{(h+E)d^2}{2048}(63\mathrm{d}\dot{e}_{j-1}-63\mathrm{d}\dot{e}_{j+1})$$
$$+\frac{\bar{c}}{32d}(33\dot{e}_{j-1}+66\dot{e}_j+33\dot{e}_{j+1})+\frac{\bar{c}}{64}(\mathrm{d}\dot{e}_{j-1}-\mathrm{d}\dot{e}_{j+1})=0 \tag{92}$$

$$\frac{Ed}{32}(3\dot{a}_{j-1}-6\dot{a}_j+3\dot{a}_{j+1})-\frac{(h+E)d^2}{2048}(-63\dot{e}_{j-1}+63\dot{e}_{j+1})-\frac{(h+E)d^3}{4096}(-27\mathrm{d}\dot{e}_{j-1}+90\mathrm{d}\dot{e}_j-27\mathrm{d}\dot{e}_{j+1})$$
$$+\frac{\bar{c}}{64}(-9\dot{e}_{j-1}+9\dot{e}_{j+1})+\frac{\bar{c}d}{128}(3\mathrm{d}\dot{e}_{j-1}-42\mathrm{d}\dot{e}_j+3\mathrm{d}\dot{e}_{j+1})=0 \tag{93}$$

in which a consistent mass matrix has been used. We can find a consistent set of harmonic solutions of the form:

$$\dot{a}_j=A\mathrm{e}^{ikx} \tag{94}$$
$$\dot{e}_j=ikB\mathrm{e}^{ikx} \tag{95}$$
$$\mathrm{d}\dot{e}_j=k^2C\mathrm{e}^{ikx} \tag{96}$$

The set of solutions at the neighbouring nodes $j\pm1$ is then:

$$\dot{a}_{j\pm1}=A\mathrm{e}^{ik(x\pm d)}=A(\cos kd\pm i\sin kd)\mathrm{e}^{ikx} \tag{97}$$
$$\dot{e}_{j\pm1}=ikB\mathrm{e}^{ik(x\pm d)}=kB(i\cos kb\pm\sin kd)\mathrm{e}^{ikx} \tag{98}$$
$$\mathrm{d}\dot{e}_{j\pm1}=k^2C\mathrm{e}^{ik(x\pm d)}=k^2C(\cos kd\pm i\sin kd)\mathrm{e}^{ikx} \tag{99}$$

Substitution of the complete solution ((94)–(99)) in the spatially discretized equations of motion (93)–(93) gives a system of three equations for which the non-trivial solution reads:

$$\omega=c_e\sqrt{\left(\frac{2}{d^2}+\frac{3k^2K_{d2}}{16}\right)\frac{(1-\cos kd)}{M_d}-\frac{kK_{d1}}{d}\frac{\sin kd}{M_d}} \tag{100}$$

Again, the parameter M_d is dependent on the mass distribution. For a consistent, a lumped and a higher-order mass matrix, respectively, we derive

$$M_d=\tfrac{1}{8}(5+3\cos kd) \tag{101}$$
$$M_d=1 \tag{102}$$
$$M_d=\tfrac{1}{16}(13+3\cos kd) \tag{103}$$

Note that (101) and (103) differ slightly from (61) and (63) because of a different location of the integration points.The values K_{d1} and K_{d2} in (100) are defined by:

$$K_{d1}=E\left(\frac{D_4}{D_2}\sin kd-\frac{3d}{16}(\cos kd-1)\right)\left(\frac{D_2}{D_2D_3-D_1D_4}\right) \tag{104}$$
$$K_{d2}=-\frac{1}{D_2}(E\sin kd+D_1K_{d1}) \tag{105}$$

with the functions:

$$D_1=k\left(\left(\frac{33\bar{c}}{16d}-\frac{135(h+E)d}{512}\right)\cos kd-\frac{33\bar{c}}{16d}-\frac{377(h+E)d}{512}\right) \tag{106}$$
$$D_2=k^2\left(-\frac{\bar{c}}{32}+\frac{63(h+E)d^2}{1024}\right)\sin kd \tag{107}$$

$$D_3 = k\left(-\frac{9\bar{c}}{32} + \frac{63(h+E)d^2}{1024}\right)\sin kd \tag{108}$$

$$D_4 = k^2\left(\left(\frac{3\bar{c}d}{64} + \frac{27(h+E)d^3}{2048}\right)\cos kd - \frac{21\bar{c}d}{64} - \frac{45(h+E)d^3}{2048}\right) \tag{109}$$

The dispersion curve of the discretized bar for a consistent mass distribution is plotted in *Figure 11a* for different sizes d of the finite element. We observe that refinement of the mesh ($d \to 0$) leads to convergence of the dispersion curve to the continuum dispersion curve. Again, we obtain an upper bound estimate for the frequency using consistent mass distribution. The influence of the mass discretization is shown in *Figure 11b*, in which a consistent, a lumped and a higher-order mass matrix have been used for a finite element with size $d = 2.0$ mm. The lumped mass matrix provides lower bound values, while the higher-order mass matrix leads to the best result as we have seen earlier for the spatially discretized strain-softening system. However, although the same tendency in accuracy between an approach with and without gradients occurs it appears that the exact order of convergence differs. In *Figure 11c*, in which ω is calculated for $k = 1.0$ 1/mm by means of (100)–(105) and ω_e is the exact frequency from the continuum dispersion analysis, we observe that the higher-order mass matrix gives the best results but does not increase the order of accuracy. So, a higher-order matrix in a gradient-dependent softening plasticity context does not imply a higher-order accuracy. Another result of the variation of mass matrices is that the type of distribution does not affect the width of a stationary localization zone. The cut-off value for wave number k and implicitly also for wave length λ is the same for the three curves in *Figure 11b*. This result is logical since inertia effects do not play a role in a stationary localization zone.

An important observation from *Figure 12*, in which the phase velocity has been plotted against the wave number, is that the point that represents the stationary localization wave ($c = 0$) gradually moves to a smaller value of k when larger elements are used. This means that the wave length ($= 2\pi/k$) which represents the width of the localization zone increases. This is exactly what is observed in numerical calculations with gradient-dependent softening plasticity models[13]. This widening of the localization band can be quantified exactly. If we take $c = 0$ in the discretized dispersion relation a dependence can be derived between the width of the localization zone in the discretized continuum w_d and the element size d. This result is plotted in *Figure 13*, in which w_d is normalized with respect to the exact width of the location zone $w_e = 2\pi l$. A criterion for the required number of finite elements n_{elem} in the localization zone can be derived. Namely, if

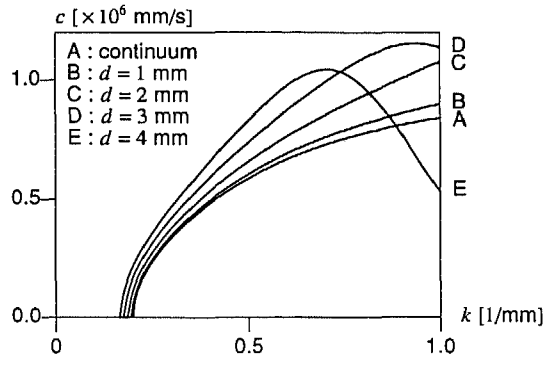

Figure 12 Dispersion curve for spatially discretized gradient-dependent softening plasticity system—real phase velocities upon variation of the finite element size using a consistent mass matrix

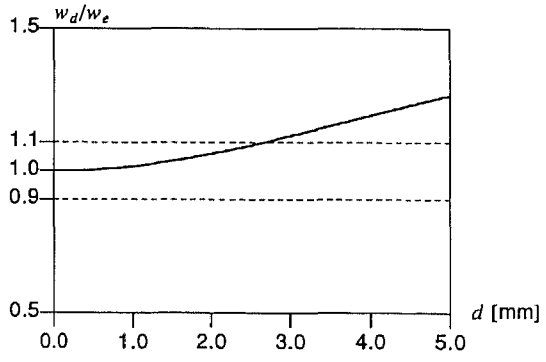

Figure 13 Spatial discretization influence on the width of the localization zone

a 10% mismatch between discretized and exact value is accepted it follows that the minimum number of finite elements is:

$$n_{\text{elem}} \geqslant \frac{w_e}{d_{\text{cri}\pm 10\%}} = 11.8 \tag{110}$$

It is noted that the use of elements with a quadratic interpolation for the velocity field results in a much less severe condition. Equation (110) is derived for a consistent mass distribution while temporal discretization effects were not considered. However, variation of the mass discretization (see *Figure 11b*) and variation of the time integration scheme (see *Figure 9a*) confirm that the wave number of the cut-off mode (and therefore the width of the localization zone) was not affected and (110) will not be different if all discretization influences would have been taken into account.

CONCLUSIONS

Temporary discretization does not affect the width of the localization zone in softening plasticity problems and gradient-dependent softening plasticity problems. Due to dissipation of energy in the softening stage lower-order modes dominate the response and discretization effects introduced by the time stepping scheme are negligible. However, a number of interesting conclusions can be drawn if higher frequency behaviour is considered. By means of an analysis of dispersive waves it is proven that a Fox–Goodwin scheme performs 4th-order accurate with respect to the time step in standard and gradient-dependent softening problems. The inclusion of numerical dissipation reduces the accuracy, except for the α method which is still 2nd-order accurate. It is noted that in localization problems the large remainder of the body is elastic and using the Fox–Goodwin method as the most accurate time-stepping scheme for the localization zone may require a small time step for the elastic part because of the conditional stability of the method.

Spatial discretization is shown to introduce additional dispersion effects which influence the formation of localization zones. In a softening plasticity continuum waves cannot propagate and do not disperse and the width of the localization zone is left unspecified. However, the numerical scheme introduces a dispersion effect by means of a dependence of the imaginary wave velocity on the wave number. The finite element solution for the localization zone appears to be a real stationary wave with a wave length set by the element size.

For a gradient-dependent softening plasticity continuum the length scale effect sets the width of the localization band. Dispersion is already a property of the material. By carrying out the dispersion analysis on the discretized system the influence of numerical dispersion on material dispersion has been determined. This leads to an accuracy criterion for the minimum number of finite elements needed in the localization zone.

Finally, the influence of mass discretization on the dispersion characteristics has been investigated. A higher-order mass matrix in a softening plasticity system is 4th-order accurate with respect to the finite element size, while consistent and lumped mass discretization show 2nd-order convergence. Also for the gradient-dependent model the higher-order mass matrix gives the best performance but does not increase the order of accuracy. The mass distribution in the finite element does not affect the width of the localization zone which is evident since inertia effects do not play a role in a localization zone which is represented by a stationary wave.

ACKNOWLEDGEMENTS

Financial support of the Royal Netherlands Academy of Arts and Sciences to the first author is gratefully acknowledged.

APPENDIX A

Lagrangian element for softening plasticity

For the linear Lagrangian element with quadrature points at $\xi=\frac{1}{2}(1\pm 1/\sqrt{3})d$ and two degrees of freedom the consistent element mass matrix reads:

$$\mathbf{M}=\rho\int_0^d \mathbf{H}^{\mathrm{T}}\mathbf{H}\,\mathrm{d}x=\frac{\rho d}{6}\begin{bmatrix}2 & 1\\ 1 & 2\end{bmatrix} \tag{A1}$$

with a cross-sectional area equal to 1. For the lumped mass matrix we have:

$$\mathbf{M}=\frac{\rho d}{2}\begin{bmatrix}1 & 0\\ 0 & 1\end{bmatrix} \tag{A2}$$

and combination of consistent and lumped mass gives:

$$\mathbf{M}=\frac{\rho d}{12}\begin{bmatrix}5 & 1\\ 1 & 5\end{bmatrix} \tag{A3}$$

representing a higher-order mass matrix. For the element stiffness matrix we use:

$$\mathbf{K}=\frac{hE}{h+E}\int_0^d \mathbf{B}^{\mathrm{T}}\mathbf{B}\,\mathrm{d}x=\frac{hE}{h+E}\frac{1}{d}\begin{bmatrix}1 & -1\\ -1 & 1\end{bmatrix} \tag{A4}$$

APPENDIX B

Hermitian element for gradient-dependent softening plasticity

For the two-noded Hermitian element with quadrature points at $\xi=\frac{1}{4}d$ and $\frac{3}{4}d$ and three degrees of freedom per node ($\dot{a}_j$, $\dot{e}_j$, $\mathrm{d}\dot{e}_j$) we use C^0-interpolants for the velocity field which gives standard definitions for **H** and **B**. For the plastic strain rates, however, we use C^1-continuous shape functions which implies:

$$\mathbf{h}^{\mathrm{T}}=\left[1-\frac{3x^2}{d^2}+\frac{2x^3}{d^3},\ x-\frac{2x^2}{d}+\frac{x^3}{d^2},\ \frac{3x^2}{d^2}-\frac{2x^3}{d^3},\ -\frac{x^2}{d}+\frac{x^3}{d^2}\right] \tag{B1}$$

and

$$\mathbf{p}^{\mathrm{T}}=\left[-\frac{6}{d^2}+\frac{12x}{d^3},\ -\frac{4}{d}+\frac{6x}{d^2},\ \frac{6}{d^2}-\frac{12x}{d^3},\ -\frac{2}{d}+\frac{6x}{d^2}\right] \tag{B2}$$

in which the conjugated vector $\dot{\mathbf{e}}=(\dot{e}_j,\mathrm{d}\dot{e}_j,\dot{e}_{j+1},\mathrm{d}\dot{e}_{j+1})$, while $\dot{\mathbf{a}}=(\dot{a}_j,\dot{a}_{j+1})$. Using **H**, **B**, **h** and **p** the element matrices in (86)–(90) can be determined, namely

$$\mathbf{M}_{aa}=\rho\int_0^d \mathbf{H}^{\mathrm{T}}\mathbf{H}\,\mathrm{d}x=\frac{\rho d}{16}\begin{bmatrix}5 & 3\\ 3 & 5\end{bmatrix} \tag{B3}$$

The lumped mass matrix is given by (A2) and the higher-order mass matrix is:

$$\mathbf{M}_{aa}=\frac{\rho d}{32}\begin{bmatrix}13 & 3\\ 3 & 13\end{bmatrix} \tag{B4}$$

The element stiffness matrices are:

$$\mathbf{K}_{aa}=E\int_0^d \mathbf{B}^{\mathrm{T}}\mathbf{B}\,\mathrm{d}x=\frac{E}{d}\begin{bmatrix}1 & -1\\ -1 & 1\end{bmatrix} \tag{B5}$$

$$\mathbf{K}_{ae}=E\int_0^d \mathbf{B}^{\mathrm{T}}\mathbf{h}^{\mathrm{T}}\mathrm{d}x=\frac{E}{2}\begin{bmatrix}-1 & -\frac{3d}{16} & -1 & \frac{3d}{16}\\ 1 & \frac{3d}{16} & 1 & -\frac{3d}{16}\end{bmatrix} \tag{B6}$$

$$\mathbf{K}_{ee}=\int_0^d[-(h+E)\mathbf{h}^{\mathrm{T}}\mathbf{h}+\bar{c}\mathbf{h}\mathbf{p}^{\mathrm{T}}]\mathrm{d}x=$$

$$-\frac{h+E}{4096}\begin{bmatrix}1508\mathrm{d} & 258\mathrm{d}^2 & 540d & -126d^2\\ 258d^2 & 45d^3 & 126d^2 & -27d^3\\ 540d & 126d^2 & 1508d & -258d^2\\ -126d^2 & -27d^3 & -258d^2 & 45d^3\end{bmatrix}+\frac{\bar{c}}{128}\frac{1}{d}\begin{bmatrix}-132 & -130d & 132 & -2d\\ -18\mathrm{d} & -21d^2 & 18d & 3d^2\\ 132 & 2d & -132 & 130d\\ -18d & 3d^2 & 18d & -21d^2\end{bmatrix} \tag{B7}$$

Note that the contribution $\mathbf{h}\mathbf{p}^{\mathrm{T}}$ introduces the non-symmetry in the stiffness matrix.

REFERENCES

1 Aifantis, E. C. On the microstructural origin of certain inelastic models, *J. Eng. Mat. Technol.*, **106**, 326–334 (1984)
2 Borst, R. de and Mühlhaus, H.-B. Gradient-dependent plasticity: formulation and algorithmic aspects, *Int. J. Num. Meth. Eng.*, **35**, 521–539 (1992)
3 Cauvern, M. Time integration schemes for wave propagation problems in linear and nonlinear media, *Graduation Thesis*, Delft University of Technology (1993)
4 Eringen, A. C. Linear theory of nonlocal elasticity and dispersion of plane waves, *Int. J. Eng. Sci.*, **10**, 425–435 (1972)
5 Eringen, A. C. Nonlocal elasticity and waves, in *Continuum Mechanics Aspects of Geodynamics and Rock Fracture Mechanics* (Ed. Thoft-Christensen), pp. 81–105, D. Reidel, Dordrecht (1974)
6 Hilber, H. M., Hughes, T. J. R. and Taylor, R. L. Improved numerical dissipation for time integration algorithms in structural dynamics, *Earthquake Eng. Struct. Dyn.*, **5**, 283–292 (1977)
7 Huerta, A. and Pijaudier-Cabot, G. Discretization influence on the regularization by two localization limiters, in *Proc. ECOMAS* (Eds. Zienkiewicz, O. C. and Oñate, E.), Brussels (1992)
8 Hughes, T. J. R. *The Finite Element Method. Linear Static and Dynamic Finite Element Analysis*, Prentice-Hall, Englewood Cliffs, NJ (1987)
9 Lasry, D. and Belytschko, T. Localization limiters in transient problems, *Int. J. Solids Structure*, **24**, 581–597 (1988)
10 Mühlhaus, H.-B. and Aifantis, E. C. A variational principle for gradient plasticity, *Int. J. Solids Structures*, **28**, 845–858 (1991)
11 Schreyer, H. L. and Chen, Z. One-dimensional softening with localization. *J. Appl. Mech.* **53**, 791–797 (1986)
12 Sluys, L. J. Wave propagation, localisation and dispersion in softening solids, *Dissertation*, Delft University of Technology (1992)
13 Sluys, L. J., Borst, R. de and Mühlhaus, H.-B. Wave propagation, localization and dispersion in a gradient-dependent medium, *Int. J. Solids Structures*, **30**, 1153–1171 (1993)
14 Sluys, L. J. and Borst, R. de Dispersive properties of gradient-dependent and rate-dependent media, *Mech. Mat.*, accepted for publication
15 Witham, G. B. *Linear and Nonlinear Waves*, Wiley, London and New York (1974)
16 Xie, Y. M. and Wood, W. L. On the accuracy of time-stepping schemes for dynamic problems with negative stiffness, *Commun. Num. Meth. Eng.*, **9**, 131–137 (1993)